



Cite this: DOI: 10.1039/c9an01176e

High-content screening Raman spectroscopy (HCS-RS) of panitumumab-exposed colorectal cancer cells†

Abdullah S. Mondol,^{‡a,b} Samir F. El-Mashtoly,^{Ⓜ‡c,d} Tatjana Frick,^{c,d} Klaus Gerwert,^{c,d} Jürgen Popp^{a,b} and Iwan W. Schie^{Ⓜ*a}

Raman spectroscopy can provide the biomolecular fingerprint of a cell in a label-free manner. Although a variety of clinical and biomedical applications have been demonstrated, the method remains largely a niche technology. The two main problems are the complexity of data acquisition and the complexity of data analysis. Generally, Raman measurements are performed manually and require a substantial amount of time. This, on the other hand, frequently results in a low number of samples and hence with questionable statistical evaluation. Here, we propose an automated high content screening Raman spectroscopy (HCS-RS) platform, which can perform a series of experiments without human interaction, significantly increasing the number of measured samples and making the measurement more reliable. The automated image processing of bright field images in combination with automatic spectral acquisition of the molecular fingerprint of cells exposed to different physiological conditions enables label-free high content screening applications. The performance of the developed HCS-RS platform is demonstrated by investigating the effect of panitumumab on SW48 and SW480 colorectal cancer cells with wild-type and mutated K-RAS, respectively, in a series of concentrations. Our result indicates that the increased content of panitumumab prohibits the activation of the MAP kinase of the colorectal cancer cells with wild-type K-RAS strongly, whereas there is no significant effect on the K-RAS mutated cells. Moreover, the relative amount of the panitumumab content present in the cells is determined from the Raman spectral information, which could be beneficial for personalized patient treatment.

Received 26th June 2019,
Accepted 26th August 2019
DOI: 10.1039/c9an01176e

rsc.li/analyst

Introduction

Raman spectroscopy allows a non-invasive and label-free assessment of the molecular fingerprint of biological samples, such as tissues and cells. Because the method measures intrinsic chemical profiles, little to no sample preparation is required, which offers a significant potential for clinical and biological applications. A variety of promising applications on eukaryotic cells, *e.g.*, drug–cell interaction,^{1–3} cell cycle analysis,⁴ and toxicology,⁵ have readily been successfully demon-

strated. While the analytical results of the approach are comparable to or even better than those of standard approaches, the transition of this analytical method from the research lab to clinical application has been stubbornly slow. This is by and large due to the complex data acquisition procedures as well as complex data processing steps, both of which require significant training. We have readily proposed a novel high-throughput screening Raman spectroscopy (HTS-RS)⁶ platform for the rapid screening and classification of subclasses and rare eukaryotic cells. The advantage in terms of throughput for the HTS-RS platform was achieved due to the automated acquisition of single spectra from an entire cell, sacrificing the information on the intracellular distribution of macromolecules obtained from Raman imaging. We have shown that we can sample tens of thousands of cells, using the HTS-RS platform by removing human dependency from the data acquisition steps. However, while the implemented approach sets new boundaries for Raman spectroscopy of eukaryotic cells, it only permits certain types of applications, *i.e.* screening applications. In many applications, *i.e.* investigation of drug–cell interactions, more than a single sample exists. The characteris-

^aLeibniz Institute of Photonics Technology, Albert Einstein str. 9, 07745 Jena, Germany. E-mail: iwan.schie@leibniz-ipht.de

^bInstitute of Physical Chemistry, Friedrich Schiller University Jena, Helmholtzweg 4, 07743 Jena, Germany

^cDepartment of Biophysics, Ruhr University Bochum, Universitätsstr. 150, 44780 Bochum, Germany

^dCenter for Protein Diagnostics (ProDi), Ruhr University Bochum, Gesundheitscampus 4, 44801 Bochum, Germany

†Electronic supplementary information (ESI) available. See DOI: 10.1039/c9an01176e

‡These authors equally contributed to this work.

ation of the efficacy of cancer therapeutics has been a promising application field for clinical Raman spectroscopy and tested for lung cancer,^{2,7} leukaemia,^{8,9} and colon cancer.^{10–12} The execution of these experiments is currently a time-consuming and tedious task, hindering the broadband screening of pharmaceutical efficacies for a large number of applications. Colorectal cancer (CRC) is one of the major causes of death¹³ and its treatment with an antigen-specific drug has been recently investigated using Raman spectroscopy.^{14,15} The effectiveness of this family of drugs, *e.g.* panitumumab (Vectibix), on colorectal cancer cells depends on the K-RAS state, which is an essential part of the MAP kinase pathway.¹⁶ The MAP kinase pathway is important because it is related to programmed cell death and other cellular activities. In general, every cell signalling pathway has some core components – a signal molecule, a receptor core kinase and messenger kinases. Epidermal growth factor (EGF) is a signalling molecule, which is responsible for cell growth, proliferation and differentiation. The EGF ligand binds to the cell membrane by means of the epidermal growth factor receptor (EGFR). Upon binding, it activates the RAS kinase – a core kinase – with the help of GRB2, SoS. The active RAS activates RAF, RAF activates MEK 1/2, MEK 1/2 activates ERK 1/2 and ERK 1/2 activates other messenger kinases, which will result in the production of transcription factor, leading to cell proliferation. Therefore, the EGFR is one of the main attractive therapeutic targets in targeted cancer therapy and this is also because the EGFR is overexpressed in 60–80% of cancers.¹⁷ Panitumumab is a fully human monoclonal antibody with a high affinity for the EGFR, which stops the activation of the MAP kinase, resulting in inhibition of cell proliferation and leading to cell death. It is approved by the U.S. Food and Drug Administration for the treatment of metastatic CRC.¹⁸ However, panitumumab was found to be effective only in CRC patients with wild-type K-RAS.¹⁹ In the case of K-RAS oncogenic mutation, which occurs in around

35–45%¹⁶ of patients with CRC, the RAS downstream signal of the EGFR is always activated and it follows the whole cell signalling pathway, independent of EGFR activation and resulting in uncontrolled cellular proliferation (Fig. 1).²⁰ As a result, a tumour will form, which will lead to cancer.¹⁹ Therefore, panitumumab therapy fails in patients with K-RAS mutated cancer. Previously the applicability of panitumumab to a cell with and without oncogenic K-RAS mutation has been demonstrated in proof of principle experiments,¹⁵ using Raman spectroscopy. Other EGFR drugs affecting RAS mutation, such as erlotinib (Tarceva), were also investigated in proof of principle experiments.¹⁴ The amount of the drug for colorectal cancer therapy can vary from one patient to another depending on the patient's weight, and the drug itself can be changed in the presence of certain oncogenic mutations such as K-RAS or BRAF mutations. As such, a platform that can accurately predict the drug efficacy in a label-free manner would greatly benefit such studies, and can further assist the treatment.

In this work, we present a novel high-content screening Raman spectroscopy (HCS-RS) platform, which allows performing an entire series of experiments, with little to no human interaction. We have previously reported on the development and application of a high-throughput screening Raman spectroscopy (HTS-RS) platform, which allowed a rapid and label-free screening for target cells in a mixture of background cells, *e.g.* identification of leukocyte subtypes and circulating tumor cells within a leukocyte background population.⁶ There is a large set of potential clinical applications that can be addressed in that manner; however, because the HTS-RS platform was designed to screen for cell types, rather to assess the underlying molecular changes induced through external factors, such as ionizing radiation or drug exposure, the set of potential applications is also limited. We have, therefore, expanded the previous concepts to enable applications where cells present in different physiological states, *i.e.* showing changes in their molecular content, can be effectively sampled. Accordingly, the newly presented platform is named high-content screening Raman spectroscopy. The performance of the HCS-RS platform for drug–cell interaction is shown in the investigation of biochemical changes in both wild-type and mutated K-RAS colorectal cancer cells *i.e.*, SW48 and SW480, respectively, at four different physiologically relevant concentrations of panitumumab. Our results indicate that panitumumab stops MAP kinase cell signalling for colorectal cancer cells with wild-type K-RAS but has no effect on mutated K-RAS cells. Moreover, the existing amount of the panitumumab content in SW48 cells can also be extracted from Raman spectra. The presented HCS-RS platform is capable of performing an entire series of experiments and acquiring a large number of spectra, resulting in stable statistical models. Furthermore, by using a multiwell cartridge, this developed platform provides more information about samples under different physiological conditions, enabling a comprehensive label-free analysis of cells, leading to a wider application of Raman spectroscopy for biomedical cell characterization.

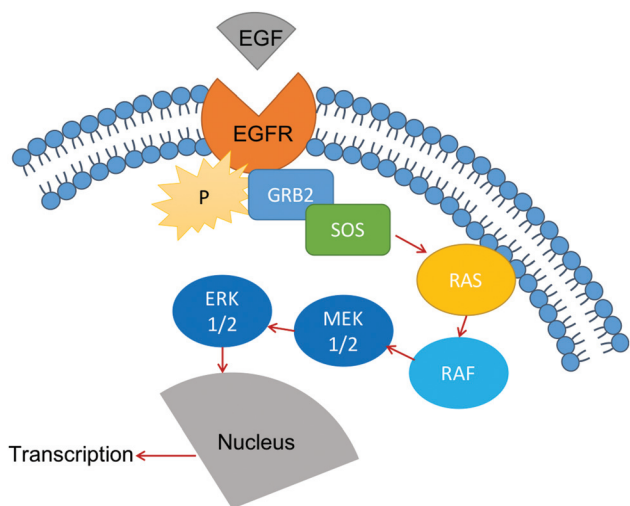


Fig. 1 The MAP kinase pathway indicating the activation of cell proliferation upon EGF reception. Panitumumab stops EGF to bind with EGFR and hence stop further steps.

Materials and methods

Cell culture

The colon cancer cell lines SW48 (CCL-231) and SW480 (CCL228) were obtained from the American Type Culture Collection. Cells were cultured in Dulbecco's modified Eagle's medium (DMEM; Invitrogen, Carlsbad, USA) supplemented with 10% fetal bovine serum (FBS; Invitrogen, Carlsbad, USA), 2 mM L-glutamine, and 5% penicillin/streptomycin, and incubated at 37 °C under a 10% CO₂ atmosphere. The cells were then seeded and grown to 80% confluence on 10 mL Petri dishes (Eppendorf) and incubated with panitumumab (1, 5, 10 and 20 µg ml⁻¹) at 37 °C in 10% CO₂ for 16 h. Subsequently, the cells were detached from the plates using trypsin/EDTA (Invitrogen, Carlsbad, USA), washed with phosphate buffered saline (PBS, Life Technologies, Darmstadt, Germany) by centrifugation and then fixed in 4% paraformaldehyde (VWR International, Darmstadt, Germany). Fixed cells were resuspended and stored in PBS.

Experimental setup

The experimental setup can be divided into four major parts based on their respective function – the excitation part, bright-field illumination, the signal collection part, and the controlling architecture. The excitation part contains the optical outline for the excitation light delivery to the sample, whereas the collection part contains the optical path to collect and to deliver the generated Raman signal to the detector. The bright field illumination is needed to locate the cells in the sample plane where the excitation and collection of the Raman signal are performed. The software ensures precise identification of the cell locations but also the switching between the different sample holder wells. The excitation section (ES) has a 532 nm LASOS DPSS laser (LASOS, Germany) excitation source, which is coupled to the system by a multimode fibre (F1) with a core diameter of 62.5 µm (Thorlabs, Germany). At the end of the fiber, a collimating lens (L1) with a focal length of 35 mm (Thorlabs, Germany) and a clean-up filter (CF) operating at 532 ± 3.7 nm at the FWHM (Semrock, Rochester, USA) are placed to collimate the incoming laser beam and to remove the unwanted background contribution generated in fiber F1. The collimated beam is directed *via* a dichroic edge filter (EF1) operating at 532 nm (Semrock, Rochester, USA) and a mirror (M1) (Thorlabs, Germany) to a 60×, NA1.0 water immersion (Nikon, Japan) objective lens (OBJ), which focuses it into the sample plane, where the laser beam diameter is approximately 10 µm. The excitation part of the system is shown by a green line in Fig. 2. The bright-field illumination path is indicated as a red line in Fig. 2. A Köhler illumination system was implemented by employing a light emitting diode (LED) with 632 nm central wavelength (Thorlabs, Germany), an iris (I) (Thorlabs, Germany), a collimating lens (L2) with 40 mm focal length (Thorlabs, Germany), and a plane mirror (M2) (Thorlabs, Germany). After illuminating the sample, the image is captured using a bright field DCC1645C-HQ CMOS camera (BF) operating in colour mode (Thorlabs, Germany), using the

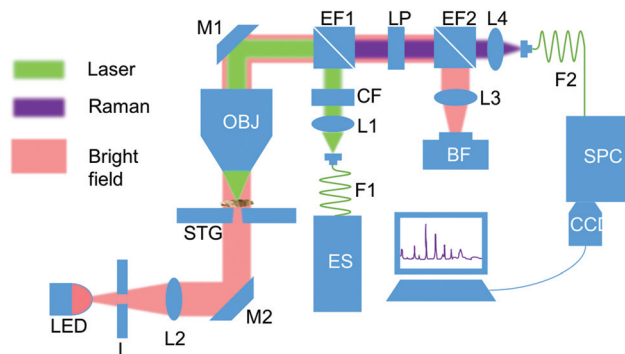


Fig. 2 Schematic of the HCS-RS system for single cell analysis. The excitation part includes ES, F1, L1, CF, EF1, M1 and OBJ, indicated by a green line. The illumination part has LED, I, L2, M2, OBJ, M1, EF1, LP, EF2, L3 and BF, indicated by a red line. The collection path includes OBJ, M1, EF1, LP, EF2, L4, F2, SPC and CCD. The automation part is realized by STG. ES – excitation source, F – fiber, L – lens, CF – clean-up filter, EF – edge filter, M – mirror, OBJ – objective, STG – xyz stages, I – iris, LP – long pass filter, BF – bright field camera, SPC – spectrograph and CCD – charged couple device.

path *via* the OBJ, mirror M1, two dichroic edge filters EF1 and EF2 (Semrock, Rochester, USA), a long pass filter (LP) (Semrock, Rochester, USA) and a focusing lens (L3) with 75 mm focal length (Thorlabs, Germany). The captured bright-field image is utilized for further analysis. During the Raman spectral acquisition, bright field illumination is always turned off. The field of view for the acquisition is 150 × 127 µm².

The collection part starts at the sample plane and ends at the cooled back-illuminated deep depletion charge couple device (CCD) camera (Pixis100, Trenton, USA). After interaction of the laser beam with the sample both Rayleigh and Raman scattering take place. The scattered light is collected by the same OBJ and reflected by mirror M1, passing dichroic edge filter EF1 and the long pass filter LP, depicted by a green line in Fig. 2. The LP allows only the Raman signal to pass and later it is focused to a 105 µm core diameter 0.12 NA multimode fiber F2 (Thorlabs, Germany), depicted in purple in Fig. 2. F2 works as a pinhole and is coupled to a spectrograph SPC (SpectraPro 2300i, Acton, USA), equipped with a 400 lines per mm grating. The dispersed beam is imaged on the CCD chip and with proper binning Raman spectra are obtained and displayed in the computer. The sample can be moved in *x-y-z*, using three linear translational stages (STG). Precise positioning in the sample space was obtained by using two CONEX-MFACC linear stages (Newport, USA) for the *XY* plane and an MTS25/M-Z8 stage (Thorlabs, Germany) for the *z*-direction, which provide a minimum step size of 0.1 µm and 1 µm precision, respectively. The samples are generally placed on CaF₂ slides (Crystal GmbH, Germany) and mounted on the motorized stages STG by means of a custom-made sample holder. The sample holder can accommodate up to six different samples, allowing six different measurements in a single run.

Development of the automated Raman platform

The automated Raman single cell analysis platform is able to perform an entire series of experiments continuously and consecutively without any user interaction. The operator has to define the number of measurement samples, the number of field of views (FoV) in each sample, and the spectral acquisition time. Then the motorized stages are used to navigate to the first sample's starting position. A pre-calibration is performed to remove the effect of small tilts of the sample holder in the x - y -plane. An auto-focus function is then employed to find the best focal plane for the Raman signal acquisition. At this point, the FoV is captured using the bright field camera and the cell detection algorithm detects the cell positions. All identified cells are probed using the excitation laser and the spectra are saved. As the SW48 and SW480 cells have comparable dimensions, *i.e.* approx. 15 μm diameter, to the laser spot size, *i.e.* approx. 10 μm diameter, a single spectrum from each cell was acquired, providing average information from the entire cell. When all cells present in the FoV are sampled, and the stage moves to the next FoV where the same process is repeated until the entire user defined FoV is completed. The approach is outlined in more detail in our previous work.⁶ As soon as one well is measured, the motorized stages move to the next well's starting position and the whole process is repeated starting from calibration to the measurement until the last FoV.

Two cell lines, SW48 and SW480, were investigated. Two wells for control cells and four wells for cells treated with four different concentrations (1 $\mu\text{g mL}^{-1}$, 5 $\mu\text{g mL}^{-1}$, 10 $\mu\text{g mL}^{-1}$, and 20 $\mu\text{g mL}^{-1}$ of panitumumab) were measured. The control cells were placed in the first and the last well, to control for time-dependent changes. A laser power of 50 mW, an integration time of 0.5 s, and 10 by 10 FoV were set as the measurement parameters.

Data analysis

To extract meaningful information, the acquired Raman spectra were pre-processed and analysed by using conventional approaches, and are described elsewhere in more detail.^{21,22} The pre-processing includes multiple steps, *i.e.* cosmic spike removal, wavelength calibration, intensity calibration, background correction, and normalization. The wavelength calibration converts the pixel value to a wavenumber value as the collected spectra have pixel numbers along with the horizontal axis. This is done by acquiring Raman spectra of acetaminophen and correlating the known peak positions to the corresponding pixel values using a polynomial fit function. Intensity calibration is performed by acquiring intensity spectra from a NIST standard white calibration lamp (Kaiser Optical System, USA) with a known emission spectrum. The intensity calibration corrects for the optical transfer function of the entire optical system, including the objective lens, the filters, and the CCD-detector. Cosmic spikes are removed by an in-house developed approach, using a combination of first and second derivative functions and linear fitting. The most

crucial part of spectral pre-processing is background correction. Extensive Multiplication Signal Correction (EMSC)²³ is one of the most common background correction methods and applied previously to process Raman spectra of cells^{4,6} and highly fluorescent tissues.²⁴ For pure components, water and cell spectra, as well as the polynomial contribution up to the second order, were included in the spectral dataset to remove unwanted background contributions. Afterwards, area normalization is performed on each of the spectra. The spectra of the two cell lines treated with different panitumumab concentrations before and after pre-processing are depicted in Fig. 3(a, c *vs.* b, d). At this point, the spectra are ready for further statistical analysis. The acquired Raman spectra were analyzed to extract meaningful information from them.

Principal component analysis (PCA) is used as a means of minimizing data dimensions, allowing obtaining relevant data from collections of complex datasets.²⁵ Spectral data are a combination of correlated variables and by applying PCA they are converted to a new set of orthogonal variables – also known as principal components (PCs). The newly generated dataset has fewer components than the original one and is organized such that the elements of the first PC account for the highest variance *i.e.*, changes in the spectral original dataset, whereas the last PC accounts for the least variance. Generally, first, several PCs provide the total variation occurring in the spectral dataset which is the most important information. The other PCs are due to the contribution of the noise. The effect of the Raman spectral change due to the molecular contributions is better understood by applying PCA to cells' Raman spectra, which hence improves the data analysis process.²⁶ The change occurring due to the panitumumab concentration can be obtained and visualized properly by applying the PCA to the spectral dataset. Later from the loadings and corresponding first two scores, the mean subtracted spectra were reconstructed to investigate the reason for cellular spectral changes due to the increased drug concentration. Using the spectral information with the known drug concentration, a partial least squares (PLS)²⁷ regression model was trained and applied to the other spectra for the prediction of the drug concentration based on the Raman spectral information.

Results

Effect of the drug concentration on cells

Although it is hard to distinguish any spectral bands from the signal acquired from both of the cell lines (Fig. 3a and c), after background correction the Raman spectral features are detectable (Fig. 3b and d). In both of the background corrected spectra, there are two controls existing as they were measured twice – before and after the drug-treated cell measurements. There was no particular spectral difference between the two control cells, which were assessed through PCA (see ESI S1, †); the second control was omitted for clarity of visualization.

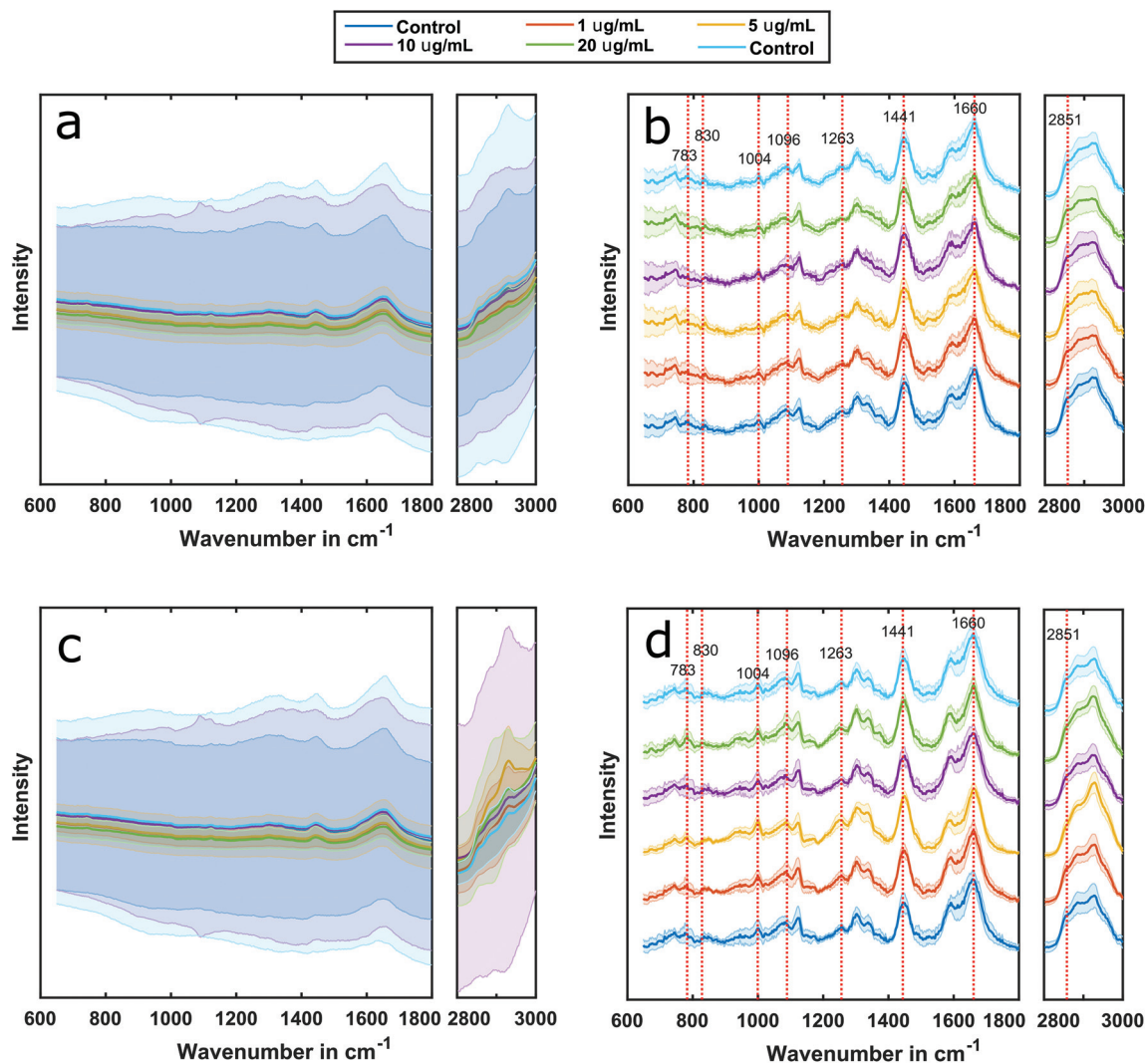


Fig. 3 The mean spectra along with the standard deviation of the acquired spectra of the SW48 (a) and SW480 (c) cells as well as their corresponding background corrected spectra (b) and (d), respectively. The mean and standard deviation of the spectra before background correction are not stacked (a and c) rather overlapped as they constitute large standard deviations. The spectra in (b and d) are offset for clarity. The control spectra were measured twice – at the beginning and at the end. The similar spectral response indicates that there is no effect of temporal shift as well as no existence of bias.

This is an indication that the temporal shift does not influence the measurement and there exists no bias from another source. Generally, the changes in the bands at 783 cm^{-1} , 813 cm^{-1} , 830 cm^{-1} and 1096 cm^{-1} correspond to the DNA U C T ring breathing, RNA O–P–O stretching, DNA B-form O–P–O asymmetric stretching and DNA PO_2 symmetric stretching, respectively, and are related to the change in nucleic acid content.^{5,28} Here the bands at 830 cm^{-1} and 1096 cm^{-1} are also due to the ring breathing of Try and chain C–C stretching respectively which is related to proteins and lipids respectively.⁵ The bands at 760 cm^{-1} representing tryptophan, 1004 cm^{-1} representing symmetric ring breathing of Phe, 1263 cm^{-1} representing amide III and 1660 cm^{-1} representing amide I are related to the change in the protein content.^{5,28} The bands at 1263 cm^{-1} and 1660 cm^{-1} correspond to =C–H

in-plane *cis* and C=C *cis* double bond stretching, respectively, which are related to lipids.²⁹ The change in lipid content is observed at 1303 cm^{-1} for C–H₂ twist,⁵ 1441 cm^{-1} for C–H scissor²⁹ and 2851 cm^{-1} for CH₂ symmetric stretching.²⁹ The bands at 1441 cm^{-1} and 2851 cm^{-1} are also present in protein spectra.⁵ The Raman spectra acquired from the SW48 cells treated with panitumumab show small changes in several spectral band positions in the background corrected spectra (Fig. 3b). On the other hand, the SW480 cells treated with different concentrations show no significant changes and all the spectra of different panitumumab treated cells exhibit similar spectral features (Fig. 3b). This is expected as the SW48 colorectal cancer cells harbour wild-type K-RAS and stop the MAP kinase activation pathway, inhibiting cell proliferation and causing some changes in cell content, which is evident in

the Raman spectra. Because the mutated SW480 cells have a K-RAS mutation, resulting in uncontrolled activation of the MAP kinase, no effects from panitumumab-treatment should be observed.

To visualize the intra-cellular changes induced through the panitumumab treatment, PCA was performed. Here, the first two components correspond to 90% of the spectral variance and the results are shown in the score plot (Fig. 4). The score values for the first two PCs of the SW48 treated cells (Fig. 4a) transit towards the negative side along both of the axes with the increase of panitumumab content – also indicated by the median value of each of the sample. The spectral changes can be understood by investigating the corresponding loading (Fig. 4b) and can be related to the macromolecular changes in the cells. The first loading of SW48 treated cells shows features at 783 cm^{-1} , 830 cm^{-1} , 1096 cm^{-1} , 1004 cm^{-1} , 1263 cm^{-1} , 1660 cm^{-1} , 1441 cm^{-1} and 2851 cm^{-1} . As the first loading resembles the lipid spectra⁹ and the lipid features are also certain, the change of lipid content is mainly responsible for

the shift in the score plot from positive to negative along PC1 in the score plot. This indicates the elevation of the lipid content in the cells with the increase of panitumumab content, where previously an increase of lipid content is observed due to the treatment with panitumumab compared to the control.¹⁵ In the second loading some negative peaks at 1441 cm^{-1} and 2851 cm^{-1} and positive peaks at 783 cm^{-1} , 830 cm^{-1} , and 1096 cm^{-1} are observed. A small contribution is also observed at 1004 cm^{-1} and 1660 cm^{-1} . These suggest a shift towards the negative side of the PC2 axis, which is mainly due to the protein and nucleic acid content. On the other hand, the changes in the score plot of SW480 treated cells spread along both of the PC1 and PC2 axes where first spreading is more significant (Fig. 4c). Here with the increase of the panitumumab content, no certain trend is observed as the spectral scores overlap with each other, which is confirmed by the overlapping median value of the different batches. The shift along PC1 is dominated by the protein and lipid change inside the cells and evident from the peaks at 1004 cm^{-1} ,

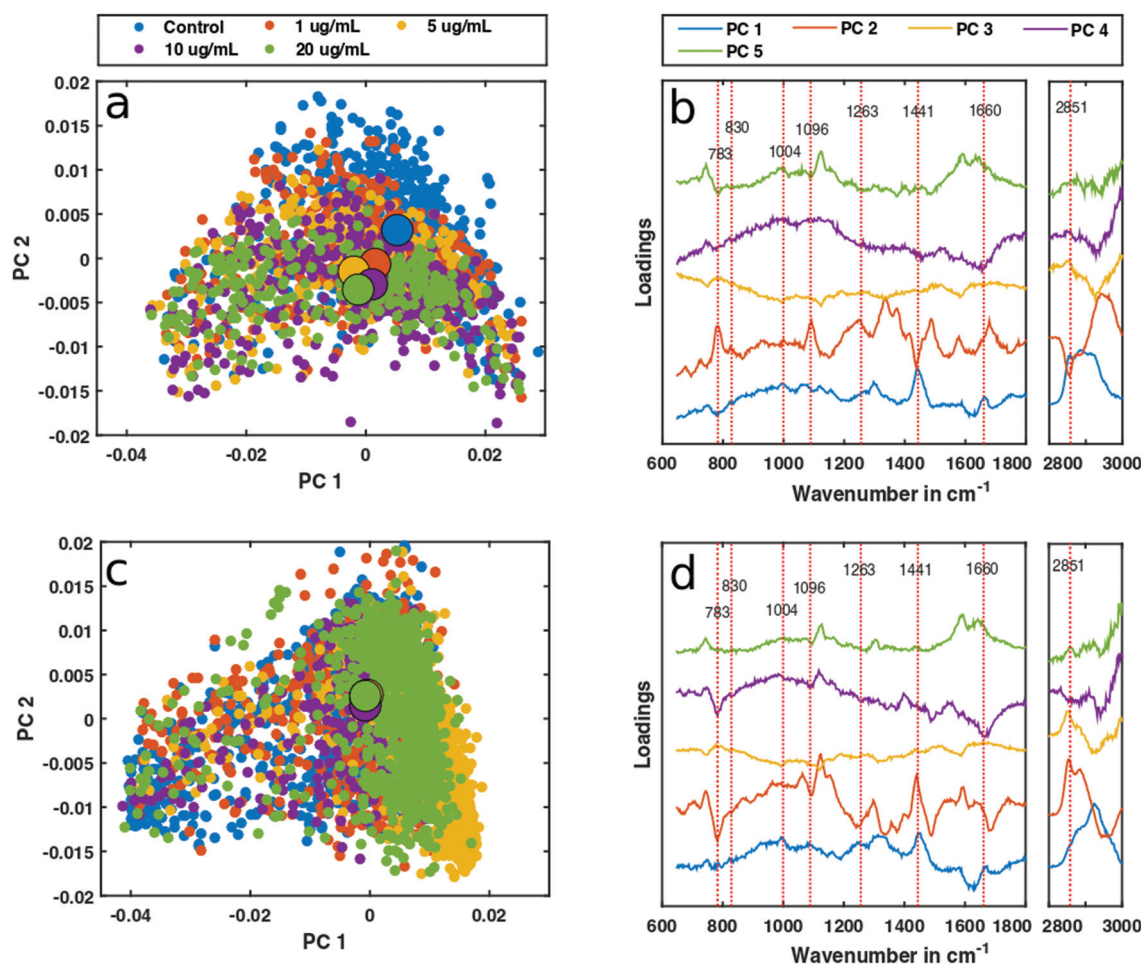


Fig. 4 The score plot of the SW48 cells (a) shows transition along both of the axes from the positive to negative sides. The transition along PC1 is due to the lipid content change which is evident in the first loadings, whereas the change along the PC2 is due to the protein and nucleic acid content of the cells (b). The score plot of SW480 overlaps on top of each other (c) and it spreads more along the PC1 axis. The spread along PC1 is mainly due to the change of protein, whereas the spreading along PC2 is due to change of lipid and nucleic acid depicted by the loading (d).

1263 cm^{-1} , and 1660 cm^{-1} in the first loading (Fig. 4d). The spread along the PC2 is mainly due to the positive peaks at 1441 cm^{-1} and 2851 cm^{-1} and negative peaks at 783 cm^{-1} , 830 cm^{-1} , and 1096 cm^{-1} , which is evident from the second loading (Fig. 4d).

Although PCA provides a convenient way to visualize the changes occurring due to the drug–cell interaction and they can be correlated with the cellular macro-molecular changes by means of the loadings, to understand the effect of panitumumab concentration on the cells as well as to understand the shift in the score plot in detail, the spectra were reconstructed from the score plot by multiplying the loadings with the corresponding scores. The average of the reconstructed spectra from the score plot for both cell lines with different panitumumab concentrations is shown in Fig. 5. They look different from the background corrected spectra (Fig. 3b and d) because the mean spectra were not added in the reconstruction process. The reconstructed spectra of the colorectal cancer cells – SW48 harbouring wild-type K-RAS, show the spectral change in a consistent way with the increase of the drug content. The peaks at 783 cm^{-1} , 830 cm^{-1} , 1096 cm^{-1} , 1004 cm^{-1} , 1263 cm^{-1} , and 1660 cm^{-1} transit from the positive to the negative direction from the control to the drug concentration increase up to 20 $\mu\text{g ml}^{-1}$ (Fig. 5). Some peaks change the sign from negative to positive, *i.e.*, 1441 cm^{-1} and 2851 cm^{-1} . The reconstructed spectra of the wild type cells show significant changes in the spectral band position or directions, *i.e.* from positive to negative (Fig. 5a), whereas the mutated cells only show small differences in the intensity, indicating that there is no drug-induced effect on the cells. It is also reflected by the overlap of the control and drug-treated cells in the score plot (Fig. 4c). In contrast, a decrease in inten-

sities is observed and the spectral features diminished most for 20 $\mu\text{g mL}^{-1}$ treatment (Fig. 5b).

Estimation of the drug concentration using Raman spectra

Up to this point using Raman spectra we could see the spectral changes due to the drug concentration for the colorectal cancer cells containing wild-type K-RAS. A proper regression model can be a powerful tool to determine the amount of drug concentration cells experience. For this, 50 spectra from each measurement were taken and their corresponding panitumumab concentration was assigned to build a PLS regression model. For the modelling, ten components were taken, which consider 94% of the spectral variance. A tenfold cross-validation was applied and a mean square error of 4.1% was obtained for the trained model. This model was then applied to the rest of the spectra to predict the treatment concentration. The mean of each predicted drug concentration is plotted and compared with the actual concentration (Fig. 6a), which shows close proximity ($R^2 = 0.9956$) in the case of SW48 cells with wild-type K-RAS.

The coefficients for PLSR show the underlying molecular fingerprint, which is correlated with the different drug concentration treatments (Fig. 6b). The coefficients are quite comparable to the PCA loadings, shown in Fig. 4b. Bands associated with nucleic acid, especially at 783 cm^{-1} and 1096 cm^{-1} , and lipid-related bands, at 1441 cm^{-1} and 1660 cm^{-1} , as well as most bands of the high-wavenumber region significantly contribute to the differences between the treatments and have previously been reported for SW48 upon EGF interaction with panitumumab.¹⁵

As panitumumab had no effect on the mutated K-RAS cancer cells, SW480, and no significant Raman spectral

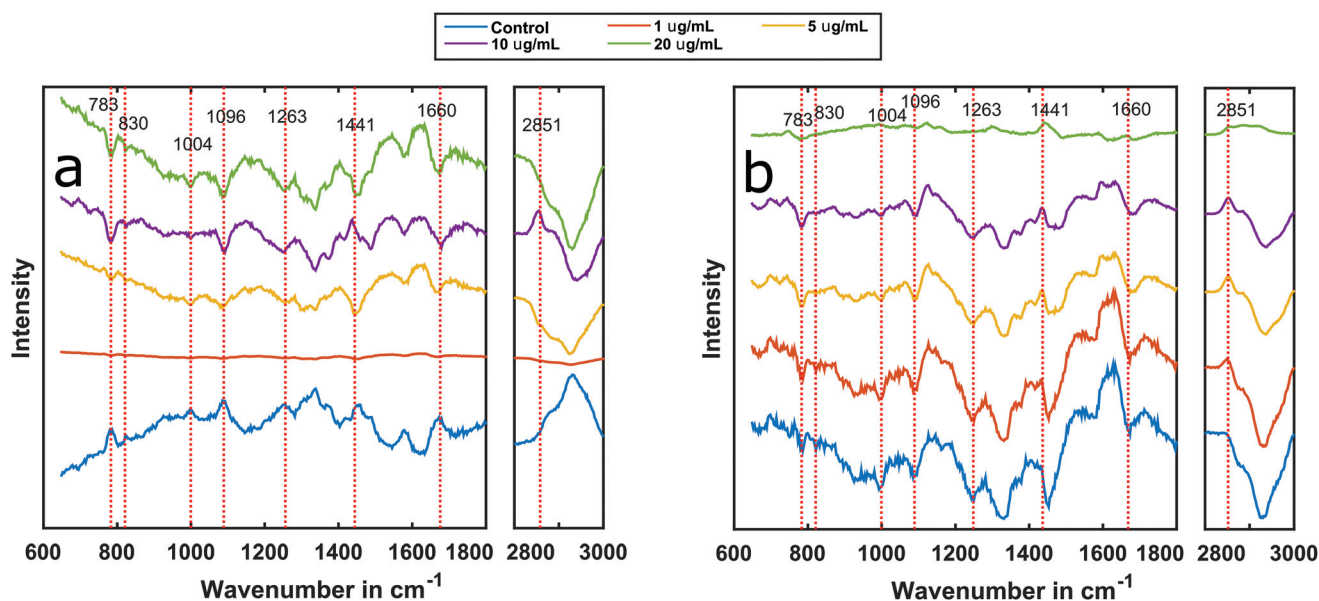


Fig. 5 The reconstructed spectra from the score plot of SW48 show significant changes with the increase of drug concentration (a); that is, Raman peaks change the direction and shape. On the other hand, the increase of drug concentration has a minimal effect on SW480 cells as the reconstructed spectra show no significant difference compared to those of the SW48 cells.

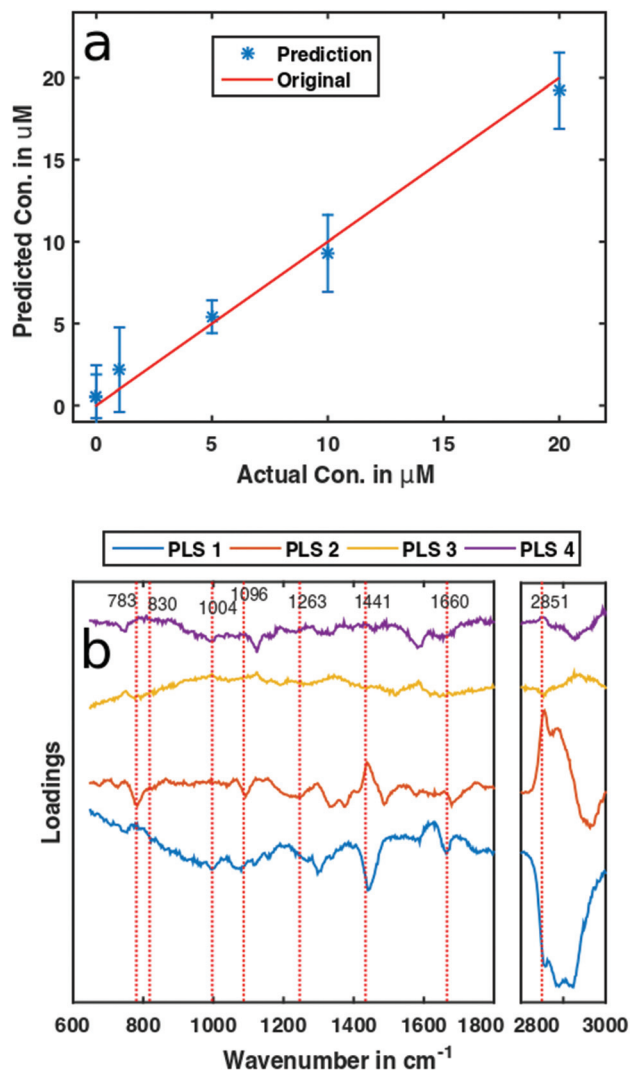


Fig. 6 The prediction of the PLS regression model shows close proximity with the actual panitumumab treatment concentration to the SW48 cells (a). The loadings of the PLS regression relate Raman spectral information to the treatment concentration of panitumumab (b). It also provides a means to estimate the drug treatment concentration from the cellular Raman signal.

change was observed, the model was not applied to relate the Raman spectral signature to the drug content.

Discussion

Here we have presented a novel high-content screening Raman spectroscopy platform, which can be used to perform an entire series of Raman experiments, without user-intervention, and enable now the screening for pharmaceutically active substances. We have shown the efficacy of the method by comparing the effects of panitumumab induced on colorectal cancer cells with and without K-RAS mutation. While previously only a handful of cells could be measured, now the approach allows measurement of thousands of cells in a label-free manner

under different conditions very rapidly. We could measure differential genotypic effects of panitumumab on wild-type colorectal cells and mutated cells. The expansion of the previously developed automated HTS-RS platform to HCS-RS, which allowed measuring a large number of cells, to assess the biomolecular fingerprint of cells without human interaction,⁶ to conduct a series of experiments fully automatically, results in a significant reduction of time and increased accuracy. In a previous study of the panitumumab interaction with SW48 and SW480, a raster scan was used to take a Raman image of the cells using 0.5 s per pixel integration time and a pixel resolution of 500 nm.¹⁵ For each batch, 50 cells were measured, which is equivalent to approximately 10 minutes for each cell measurement and 8.5 hours for a batch measurement which could be longer if human interaction is accounted for. For the conducted study of this work, this method would require a minimum of 102 hours or more than 4 days to probe 600 cells from 12 batches. The experiments conducted using the HCS-RS platform in this study have an integration time of 0.5 s per cell and a delay due to the stages, approximately 0.4 s, which enables measurement of a minimum of 1000 cells in 15 min, resulting in 3 hours of experiment with a minimum 12 000 cell spectral dataset. The HCS-RS platform is faster due to the integration of process automation which consists of cell detection, translation to the cell position, automated z-calibration, spectral acquisition, saving, *etc.* This approach will ultimately lead to the expansion of Raman spectroscopy as a tool for a fast *in vitro* analysis of drug influence for patient-specific personalized cancer treatment.

The acquisition of a Raman spectrum from a random cellular location can result in high spectral variations, as a single spectrum is acquired from each of the cells provides the local cellular macromolecular content information, and it is difficult to indicate the representativeness of the spectrum. This is overcome by acquiring spectra with an extended optical probing beam, which provides the average information of the cellular content faster than, for example, taking an image and hence facilitates the measurement of a substantial number of cells in a brief time period. The minimum amount of spectra needed for obtaining average cell information is demonstrated in ref. 30. Although it is difficult to distinguish a change in Raman bands from the background corrected spectra (Fig. 3b), usage of proper multivariate analysis tools can detect drug-related changes in cells. Clearly, a consistent trend is observed with the increase of panitumumab concentration for the SW48 cell lines (Fig. 4a). Reconstructed spectra from the score plot also (Fig. 5a) indicate the reason behind the change strongly by means of altering the peak direction, which is related to the cellular macro-molecular change, *i.e.* proteins, lipids and nucleic acids. This is an indication that with the increase of the drug concentration, the prohibition of ligand binding to the extracellular receptor is increased and the MAP kinase activation is hampered more strongly, which results in increased apoptosis and cell proliferation inhibition. On the other hand, the random overlaps of the scores in the score plot for the SW480 cell line (Fig. 4c) indicate no influence of the increased

drug concentration on the K-RAS mutated colorectal cells. This is also confirmed using the reconstructed spectra (Fig. 5b), as they show non-significant differences from each other. The results support the knowledge that for the mutated colorectal cancer cells, increased drug concentrations cannot prohibit MAP kinase activation as they are always activated due to the mutation and have no effect due to the therapeutic treatment. The *in vitro* results of SW48 and SW480 cells are in agreement with the clinically observed patient responses to panitumumab therapy.^{16,31}

In the end, the cellular drug content for the wild-type K-RAS colorectal cancer cells could be estimated based on Raman spectra using the PLS regression model. This enables semi-quantification of the drug concentration based on the intracellular changes (Fig. 6a), providing an interesting prospect for therapy-response monitoring.

Conclusions

The expansion of the high-throughput screening Raman spectroscopy platform to a high-content screening Raman spectroscopy platform enables not only sampling of a large number of cells but also allows performing high-content screening experiments using Raman spectroscopy in a short period of time and in a fully automated fashion. The acquisition of a significant number of spectra is important for establishing proper statistical modelling. Based on acquired Raman spectra the changes in the cellular macromolecular content can be observed and can be related to the cell signalling pathways. Moreover, the existing drug content in the cells could also be estimated based on the spectral signature. Our experiment demonstrates that *in vitro* Raman spectroscopy combined with automation provides statistically viable results, making it a complementary, easy-to-use tool for bio-lab and clinical applications.

Conflicts of interest

The authors declare that there is no conflict of interest.

Acknowledgements

This research was supported by the Protein Research Unit Ruhr within Europe (PURE), Ministry of Innovation, Science, and Research (MIWF) of North-Rhine Westphalia, Germany, and European Regional Development Fund, European Union and North-Rhine Westphalia, Germany.

Notes and references

- Z. Farhane, F. Bonnier and H. J. Byrne, *Anal. Bioanal. Chem.*, 2016, **409**, 1333–1346.
- Z. Farhane, F. Bonnier, O. Howe, A. Casey and H. J. Byrne, *J. Biophotonics*, 2017, **14**, 1–14.
- P. C. Ortiz-Lazareno, A. Bravo-Cuellar, J. M. Lerma-Díaz, L. F. Jave-Suárez, A. Aguilar-Lemarroy, J. R. Domínguez-Rodríguez, O. González-Ramella, R. De Céelis, P. Gómez-Lomelí and G. Hernández-Flores, *Cancer Cell Int.*, 2014, **14**, 1–14.
- K. Eberhardt, C. Beleites, S. Marthandan, C. Matthäus, S. Diekmann and J. Popp, *Anal. Chem.*, 2017, **89**, 2937–2947.
- I. Notinger, *Sensors*, 2007, **7**, 1343–1358.
- I. W. Schie, J. Rüger, A. S. Mondol, A. Ramoji, U. Neugebauer, C. Krafft and J. Popp, *Anal. Chem.*, 2018, **90**, 2023–2030.
- M. K. Hammoud, H. K. Yosef, T. Lehtonen, K. Aljakouch, M. Schuler, W. Alsaïdi, I. Daho, A. Maghnouj, S. Hahn, S. F. El-Mashtoly and K. Gerwert, *Sci. Rep.*, 2018, **8**, 1–11.
- T. J. Moritz, D. S. Taylor, D. M. Krol, J. Fritch and J. W. Chan, *Biomed. Opt. Express*, 2010, **1**, 1138.
- I. W. Schie, L. Alber, A. L. Gryshuk and J. W. Chan, *Analyst*, 2014, **139**, 2726–2733.
- E. Heister, V. Neves, C. Tilmaciu, K. Lipert, V. Sanz Beltran, H. M. Coley, S. R. P. Silva and J. McFadden, *Carbon*, 2009, **47**, 2152–2160.
- N. Yadav, A. Pliss, A. Kuzmin, P. Rapali, L. Sun, P. Prasad and D. Chandra, *Cell Death Dis.*, 2014, **5**, e1453–e1412.
- H. K. Yosef, T. Frick, M. K. Hammoud, A. Maghnouj, S. Hahn, K. Gerwert and S. F. El-Mashtoly, *Analyst*, 2018, **143**, 6069–6078.
- R. Siegel, K. D. Miller and J. Ahmedin, *CA Cancer J. Clin.*, 2017, **67**, 7–30.
- H. K. Yosef, L. Mavarani, A. Maghnouj, S. Hahn, S. F. El-Mashtoly and K. Gerwert, *Anal. Bioanal. Chem.*, 2015, **407**, 8321–8331.
- S. F. El-Mashtoly, H. K. Yosef, D. Petersen, L. Mavarani, A. Maghnouj, S. Hahn, C. Kötting and K. Gerwert, *Anal. Chem.*, 2015, **87**, 7297–7304.
- A. Bardelli and S. Siena, *J. Clin. Oncol.*, 2010, **28**, 1254–1261.
- K. Inamura, H. Ninomiya, Y. Ishikawa and O. Matsubara, *Arch. Pathol. Lab. Med.*, 2010, **134**, 66–72.
- S. B. Patel, D. Gill and I. Garrido-laguna, *OncoTargets Ther.*, 2015, **9**, 75–86.
- F. Petrelli, K. Borgonovo, M. Cabiddu, M. Ghilardi and S. Barni, *Int. J. Colorectal Dis.*, 2011, **26**, 823–833.
- A. I. Phipps, D. D. Buchanan, K. W. Makar, A. K. Win, J. A. Baron, N. M. Lindor and J. D. Potter, *Br. J. Cancer*, 2013, **108**, 1757–1764.
- K. Eberhardt, C. Stiebing, C. Matthäus, M. Schmitt and J. Popp, *Expert Rev. Mol. Diagn.*, 2015, **15**, 773–787.
- T. Dörfer, T. Bocklitz, N. Tarcea, M. Schmitt and J. Popp, *Z. Phys. Chem.*, 2011, **225**, 753–764.
- N. K. Afseth and A. Kohler, *Chemom. Intell. Lab. Syst.*, 2012, **117**, 92–99.
- E. Cordero, F. Korinth, C. Stiebing, C. Krafft, I. W. Schie and J. Popp, *Sensors*, 2017, **17**, 1724–1741.
- H. Abdi and L. J. Williams, *Wiley Interdiscip. Rev. Comput. Stat.*, 2010, **2**, 433–459.
- F. Bonnier and H. J. Byrne, *Analyst*, 2012, **137**, 322–332.

- 27 R. D. Tobias, SAS Conf. Proc. SAS Users Gr. Int. 20 (SUGI 20), 1995, pp. 2–5.
- 28 Z. Farhane, F. Bonnier, A. Casey and H. J. Byrne, *Analyst*, 2015, **140**, 4212–4223.
- 29 M. C. Potcoava, G. L. Futia, J. Aughenbaugh, I. R. Schlaepfer and E. A. Gibson, *J. Biomed. Opt.*, 2014, **19**(11), 111605.
- 30 I. W. Schie and J. W. Chan, *J. Raman Spectrosc.*, 2016, **47**, 384–390.
- 31 R. G. Amado, M. Wolf, M. Peeters, E. Van Cutsem, S. Siena, D. J. Freeman, T. Juan, R. Sikorski, S. Suggs, R. Radinsky, S. D. Patterson and D. D. Chang, *J. Clin. Oncol.*, 2007, **26**, 1626–1634.